Environmental Science Nano

ROYAL SOCIETY OF CHEMISTRY

PAPER

View Article Online
View Journal

Check for updates

Cite this: DOI: 10.1039/d3en00633f

Published on 05 December 2023. Downloaded by Duke University on 12/13/2023 5:24:52 PM.

Balancing functional properties and environmental impact of graphitic carbon nitride: a case study on boron doping syntheses†

Yash Shah [ac] and Leanne M. Gilbertson *[abc]

Graphitic carbon nitride (g-CN) possesses properties that make it suitable for various applications, including photocatalysis, carbon dioxide reduction, sensing, water-splitting, and nitrogen fixation. To overcome performance limitations arising from limited visible-light absorption and rapid recombination of photo-induced charge carriers, we employ heteroatom doping in a minimally impactful manner. Boron as a dopant is chosen due to its electron deficiency compared to carbon and nitrogen, enabling the replacement of either element in the g-CN backbone and influencing the optical properties of boron-doped carbon nitride (BCN). Our investigation reveals that the replacement of carbon atoms by boron within the g-CN framework influences the BCN's optical bandgap, 1.67 eV to 2.52 eV, and effectively modulates electron–hole recombination. Further, using different synthesis approaches and boron precursors results in vastly different material morphology. The boron-doping-induced structural defects lead to bandgap energy reduction. However, we find that this reduction does not correlate with the suppression of electron–hole recombination. In addition to studying physicochemical properties that underline BCN functional performance across a wide range of energy and environmental applications, we compare the environmental impacts across the multiple BCN syntheses. This assessment encompasses a comparison across nine TRACI midpoint impact categories, such as global warming potential, human health impacts from carcinogenic and noncarcinogenic substances, and ecotoxicity. Our life cycle impact assessment results demonstrate that electricity is the major contributor to the overall impacts of BCN synthesis, regardless of the synthesis technique used. Further, we propose a MAPS (Material Properties and Sustainability) evaluation approach that simultaneously considers physicochemical properties and sustainability metrics to gain valuable insights into designing minimally impactful, high-performing carbon nitride materials.

Received 12th September 2023,
Accepted 4th December 2023

DOI: 10.1039/d3en00633f

rsc.li/es-nano

Environmental significance

Graphitic carbon nitride is a 2D nanomaterial that has emerged as a promising material to address challenges pertaining to water contamination, carbon emissions, and energy production. Its properties as a visible light photocatalyst hold immense value, yet controlling its properties to achieve adaptability and sustainability remains unrealized. This study uncovers ways to tune optical and chemical characteristics of carbon nitride through boron doping and diverse synthesis methods. The work also introduces an approach to harmonize physicochemical characteristics with sustainability benchmarks at the material synthesis stage. By considering both dimensions in tandem, design of graphitic carbon nitride is pursued for high-performing properties while minimizing its environmental footprint.

1.0 Introduction

Nanotechnology underpins technological advances of tomorrow with wide-ranging impacts in the fields of electronics and computing, healthcare, energy and environment, material science, and manufacturing. However, the versatile functionality of nanotechnology demands complementary research on the environmental impact, health and safety risks, and scalable transitioning from lab-scale to large-scale production of nanomaterials. With the global nanotechnology market projected to reach an impressive USD 23.6 billion by

[a] Department of Civil and Environmental Engineering, University of Pittsburgh, Pittsburgh, 15206, USA
[b] Department of Chemical and Petroleum Engineering, University of Pittsburgh, Pittsburgh, 15206, USA
[c] Department of Civil and Environmental Engineering, Duke University, Durham, 27708, USA. E-mail: leanne.gilbertson@duke.edu

† Electronic supplementary information (ESI) available. See DOI: https://doi.org/10.1039/d3en00633f

Published on 05 December 2023. Downloaded by Duke University on 12/13/2023 5:24:52 PM.

2026,[1] it is imperative to investigate the emerging physicochemical properties of nanomaterials alongside the corresponding environmental impact of the processes involved in their synthesis and manufacturing.

Graphitic carbon nitride (g-CN) is a promising nanomaterial with expanding applications due to its favorable physicochemical properties,[2] such as metal-free composition,[3] tunable structure,[4,5] biocompatibility,[6] chemical inertness,[7] and visible-light response.[8–10] The current and future applications of carbon nitride span photocatalysis,[3,7,9] hydrogen generation,[11–13] carbon dioxide reduction,[7] and sensing.[4] In its pristine form, carbon nitride suffers from a few drawbacks, such as limited bandgap for visible-light absorption and rapid recombination of photo-induced electron–hole pairs.[8] Collectively, these drawbacks negatively influence the charge transfer and generation of radical oxidative species, which are crucial for carbon nitride's efficacy in the above-listed applications.

There are several approaches to improve g-CN properties, including doping with metals/non-metals,[5] synthesizing nanocomposites with graphene,[14–16] and surface functionalization.[17,18] Among the suggested approaches, elemental doping with heteroatoms is considered an effective strategy to modulate the optical and electronic properties of carbon nitride.[5,19] Heteroatom doping is a promising approach since it is metal-free, allows adjustment of visible-light activation, and enhances catalytic activity due to modification of the g-CN electronic structure and surface properties.[5,20] In this study, we investigate boron atom doping because boron is a p-type semiconductor dopant that can introduce positive charge carriers into the g-CN framework to facilitate the flow of electric current.[21,22] Moreover, boron has also been found effective in regulating the band structure[23–25] that can influence the light absorption and emission characteristics of g-CN. This motivates us to evaluate the optimal amount of B that could be doped into the g-CN framework, its influence on the optical and electronic properties, and its correlation with various boron-doped carbon nitride (BCN) synthesis approaches.

There are various strategies to synthesize graphitic carbon nitride and BCN, with supramolecular and non-supramolecular approaches being widely popular. The supramolecular approach of synthesis involves molecular self-assembly of melamine and cyanuric acid and has demonstrated improved local order, charge separation, and electrical conductivity for g-CN.[26,27] The non-supramolecular (NS) approach involves direct calcination of g-CN precursors such as melamine, urea, and dicyandiamide.[25,28,29] While both approaches to molecular assembly have been pursued, there remains an opportunity to realize how the synthesis approach influences BCN physicochemical properties. Herein, we report a methodology we developed that adopts the supramolecular approach for BCN synthesis using boric acid. In addition, we synthesize BCN using the NS approach with two different boron precursors, boric acid and ammonia borane. Given the diverse strategies for synthesizing BCN and the range in resultant physicochemical properties, we take the opportunity to demonstrate how we couple material design with environmental impact assessment, using life cycle assessment (LCA), providing guidance on sustainable BCN development. This investigation into BCN physicochemical properties that emerge from different synthesis approaches, in conjunction with a sustainability assessment of the associated BCN production, demonstrates a unique methodology that we propose to importantly inform the future development of a promising visible light photocatalyst in its wide-ranging applications.

2.0 Experimental

2.1. Chemicals

Boric acid (BA, 99%), cyanuric acid (CA, 98%), and dicyandiamide (DCDA, 99%) were purchased from Sigma-Aldrich (St. Louis, MO). Melamine (M, 99%) and borane-ammonia complex (AB, >85%), ethanol (190 proof), were purchased from Acros Organics B.V.B.A. (Geel, Belgium), TCI chemicals (Tokyo, Japan), and Decon Labs Inc. (King of Prussia, PA), respectively. All reagents employed in the synthesis were used without further purification.

2.2. Synthesis of the supramolecular boron-doped carbon nitride (S-BCN) sample set

X mmol (*X* = 0, 1, 2, 3) of BA was stirred at 600 rpm with 1 g of melamine and 1.02 g of cyanuric acid (M : CA molar ratio = 1 : 1) in a parafilm-covered beaker with 40 ml ethanol for 3 h at room temperature. Next, the mixture was sonicated inside the same beaker using a bath sonicator (Aquasonic Model 150HT) for 1 h. Subsequently, the sonicated mixture was dried overnight at 80 °C. After drying, the resultant powder was ground using mortar and pestle and transferred to a quartz crucible for calcination inside the muffle furnace (Thermo Scientific Lindberg/Blue M TF55035A-1). The muffle furnace was heated to 500 °C with a ramp rate of 2.5 °C min^{-1}. Once the maximum temperature was reached, the powder sample was calcined for 3 h under the N_2 (prepurified gas 99.9985%, Matheson UN1066) gas flow (rate 100 mL min^{-1}), after which the furnace was turned off and cooled naturally. After reaching room temperature, the crucible was removed, samples were weighed, and stored in glass vials in the dark. The yield obtained for this synthesis scheme was 24.03%.

2.3. Synthesis of the non-supramolecular boron-doped carbon nitride from boric acid (NS-BCN-BA) sample set

BCN was synthesized based on the approach demonstrated by Peng *et al.*[25] Briefly, *X* mmol (*X* = 0, 1, 2, 3, 6) of BA was stirred at 600 rpm with 1 g of melamine in a beaker with 10 ml deionized (DI) water for 3 h at room temperature. The mixture was dried overnight at 100 °C. The resultant powder was ground using mortar and pestle and transferred to an alumina crucible for calcination inside the muffle furnace

 This journal is © The Royal Society of Chemistry 2023

Published on 05 December 2023. Downloaded by Duke University on 12/13/2023 5:24:52 PM.

(*vide supra*). The muffle furnace was heated to 550 °C at a ramp rate of 5 °C min^{-1}. The powder was calcined for 4 h at 550 °C under the Air (zero gas, Matheson UN1002) gas flow (rate 100 ml min^{-1}), after which the furnace was turned off and was cooled naturally. The powder sample was collected from the crucible, washed with water while on filter paper, dried, ground, and stored in glass vials in the dark. The yield achieved for this synthesis method was 61.30%.

2.4. Synthesis of the non-supramolecular boron-doped carbon nitride from ammonia borane (NS-BCN-AB) sample set

BCN was synthesized from ammonia borane following the method by Wang *et al.*[30] Briefly, *X* g (*X* = 0, 0.02, 0.1, 0.2, equivalent to 0, 0.64, 3.20, and 6.40 mmol, respectively) of AB was added to 10 ml deionized water in a beaker and stirred for 5 min (note: mass, g, was used instead of mmol to keep the synthesis consistent with Wang *et al.* approach.). After stirring, 2 g of DCDA was added to the aqueous solution and stirred for 1 h at 600 rpm and room temperature. The mixture was heated at 100 °C overnight to evaporate the solvent. The resultant powder was then ground using mortar and pestle and transferred to a quartz crucible for calcination inside the muffle furnace. The calcination was carried out at 600 °C (ramp rate of 2.39 °C min^{-1}) for 4 h under N_2 gas flow (rate 100 ml min^{-1}), after which the furnace was turned off and cooled to room temperature naturally. The calcined powder was ground and stored in glass vials in the dark. The yield observed for this synthesis technique was 21.78%.

2.5. Material Characterization

Powder X-ray diffraction (XRD) was used to confirm the crystal structure of graphitic carbon nitride. Samples were analyzed using a Bruker D8 Discover instrument (Cu Ka, 40 kV, 40 mA). The chemical compositions of the synthesized BCN samples were analyzed by X-ray photoelectron spectroscopy (XPS) using an ESCALAB 250Xi (Thermo Scientific) instrument with a monochromatic Al Ka X-ray source (1486.7 eV, spot size of 650 mm). Optical band gap data were collected with a LAMBDA-750 UV-vis-NIR spectrophotometer (PerkinElmer L750) equipped with a 60 mm integrating sphere using barium sulfate as the standard reference. Steady-state photoluminescence (ss-PL) was used to determine the charge separation efficiency of BCN samples. Spectra were measured on a FluoroMax-3 spectrometer (Jobin Yvon Horiba) with excitation at carbon nitride's characteristic excitation wavelength of 330 nm.[31] Transmission electron microscopy (TEM) imaging with electron energy loss spectroscopy (EELS) for elemental mapping was performed on a JEOL JEM-2100F TEM instrument operated at 200 kV. Sample preparation for all the characterization techniques has been discussed in the ESI† (Section S1).

2.6. Sustainability Assessment of Syntheses

2.6.1. Scope, System Boundary, and Functional Unit. A cradle-to-gate life cycle impact assessment was conducted for the three BCN syntheses. This includes all inputs, emissions, and transportation associated with raw material acquisition through the production of the BCN (*e.g.*, upstream resource extraction, energy required for producing reagents, and direct emissions from energy generation). We adopted a mass-based functional unit of one gram of BCN synthesized, instead of a performance-based functional unit, for two reasons: (i) the focus of this work and intended use of the life cycle assessment results is to inform material synthesis-property tradeoffs, and (ii) BCN is proposed for use in many energy and environmental applications (*e.g.*, water disinfection, water splitting, biosensing, carbon dioxide reduction), each having distinct use cases and thus, different associated functional units. Our intent is to remain as broadly applicable as possible, and the mass-based functional unit is most transferrable to future studies and other researchers.

2.6.2. Impact assessment. A life cycle impact assessment was conducted on the three BCN synthesis routes described above (refer to Section S2 and Tables S1–S5† for the inventory details of each synthesis route). The impact assessment was performed using SimaPro 9.1 (PRé Consultants). The United States Life Cycle Inventory (USLCI)[32] was chosen when available; otherwise, Ecoinvent 3 was selected.[32–34] Environmental impacts were modeled using the United States Environmental Protection Agency's Tool for the Reduction and Assessment of Chemical and Other Environmental Impacts (TRACI) 2.1 assessment method.[35] Environmental impact categories include global warming potential (GWP, in kg CO_2 eq), photochemical smog formation (PS, in kg O eq), acidification (AC, kg SO eq), eutrophication (EU, kg N eq), human health impacts from toxic carcinogenic (HHC) and noncarcinogenic (HHNC) substances (in comparative toxic units for human toxicity impacts, or CTUh), respiratory effects (RE, in kg PM2.5 eq), ecotoxicity (EC, in comparative toxic units for aquatic ecotoxicity impacts, or CTUe), and fossil fuel depletion (FF, in MJ surplus).

2.6.3. Uncertainty analysis. Uncertainty analysis was performed using Monte Carlo simulation (1000 runs, SimaPro 9.1) to assess the uncertainty of the cumulative unit process life cycle inventory data associated with each synthesis route. For unit processes available in the selected databases (*i.e.*, USLCI, Ecoinvent), the default lognormal distributions were used. For unit processes created by the authors, the uncertainty factors are calculated for each input and output data considering a lognormal distribution and utilizing the Pedigree matrix approach (refer to Section S3 and Tables S1–S5† for uncertainty plots and for the standard deviations generated using pedigree matrix approach, respectively).

3.0 Results and Discussion

3.1. Modulating boron doping of carbon nitride

3.1.1. Confirming the characteristic tri-*s*-triazine structure formation. Density functional theory studies demonstrate that the tri-s-triazine structure (Fig. 1) is the most stable among all the allotropes of g-CN, and thus, it is recognized

Published on 05 December 2023. Downloaded by Duke University on 12/13/2023 5:24:52 PM.

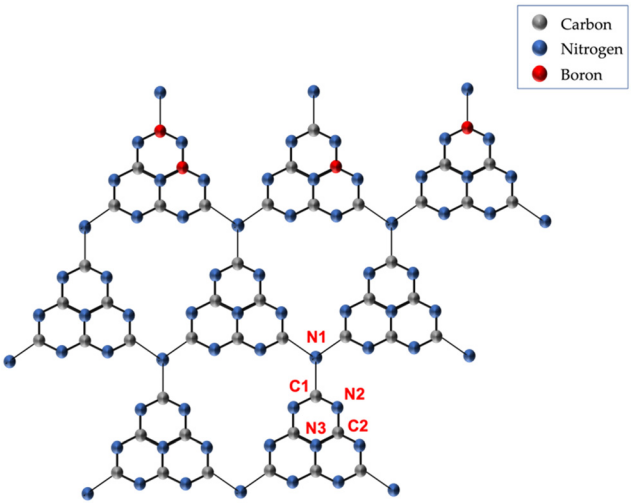

Fig. 1 The tri-*s*-triazine structure for graphitic carbon nitride with possible boron doping sites indicated (red atoms).

as its fundamental building block.[36,37] The tri-*s*-triazine structure consists of three nonequivalent nitrogen atoms (N1, N2, N3) and two nonequivalent carbon atoms (C1, C2). We employed X-ray photoelectron spectroscopy (XPS) to verify the presence of the tri-*s*-triazine bonding moieties. The C 1s spectra of all synthesized BCN samples (shown in Tables S6–S8† under the C 1s column) exhibit peaks at 284.4 eV (C–C), representing adventitious carbon impurities introduced during synthesis and XPS sample preparation.[38,39] Additionally, peaks were observed at 288 eV (C1–N2═C2),[27,30,40] along with some peaks above 290 eV identified as satellite peaks.[27] The N 1s BCN spectra (shown in Tables S6–S8† under the N 1s column) show peaks at 398.5 eV (C1–N2═C2),[30,31,38] 399.5 eV (N–H, pyrrolic nitrogen),[36,37] and 400.1 eV (N3, graphitic),[36,37] along with peaks above 401 eV, which were identified as satellite peaks.[41,42] The presence of satellite peaks (in the N 1s spectra) indicates the phenomenon of pi–pi electron excitation, characteristic of the pi-conjugated structure in the tri-s-triazine ring of g-CN.[43] Thus, regardless of the synthesis approach adopted, XPS indicates the attainment of the tri-s-triazine backbone.

3.1.2. The extent of boron doping varies with the synthesis approach. The boron doping atomic percentages were determined using XPS as the average of three different locations on the BCN sample (refer to Section S1† for sample preparation and characterization details). The synthesis-specific boron atomic percentages are listed in Table 1. Interestingly, when the same amount of dopant (molar ratio) was used during synthesis, significantly lower B atomic percentages were observed for the SBCN samples compared to the NSBCN-BA samples. Shalom *et al.* show that during the SBCN synthesis, the formation of the melamine-cyanuric acid complex as an intermediate is stabilized by hydrogen bonds.[26] This stabilization can have two effects: (i) allowing fewer boron atoms to enter the tri-*s*-triazine framework, and/or (ii) exposing fewer melamine molecules to react with boron atoms. These factors could lead to the lower observed boron doping in the SBCN samples (Table 1).

3.1.3. Boron replaces carbon atoms in the tri-*s*-triazine structure. The B 1s peak deconvolution reveals a single peak in the range of 191.7–192.2 eV in all samples (Fig. 2) corresponding to B–N bonds.[25,44] This observation indicates that the B atom replaces the C atom (Fig. 1) (note: it remains unclear if the replaced C atom(s) were C1, C2, or both because XPS only confirms the presence of the B–N bond in the B 1s spectra and cannot resolve the location-specific differences for similarly hybridized atoms) in the g-CN tri-*s*-triazine structure. The broader and less intense peak observed in the SBCN sample (Fig. 2a) could be a result of lower boron doping (see Table 1). Additional peaks were observed at 188 eV and 197 eV, particularly for the NSBCN-AB (Fig. 2c) samples. A previous study[45] suggests that the B 1s peak at 188 eV represents B–C bonds. Since this B–C peak is observed in the highest doped sample of the NSBCN-AB sample set (B atomic % = 17.41, in the case of 6.4 mmol NSBCN-AB), it is possible that boron is replacing some nitrogen atoms in the g-CN framework. A 6 mmol NSBCN-BA sample was synthesized to investigate whether a similar trend was observed with an increase in doping and for the presence of a B–C peak. The same trend was not observed, nor was the B–C peak (Table S7,† B 1s column). We believe this difference emerged from the use of different precursors (melamine and boric acid *versus* dicyandiamide and ammonia borane) involved in the NSBCN-BA synthesis. The peak at 197 eV is possibly a satellite peak,[46] resulting from shake-ups, energy loss, plasmons, and electron excitation.

3.2. Boron atoms distort the interlayer stacking

The crystal structure of the synthesized samples was investigated using XRD. The obtained diffractograms for the

Table 1 Boron doping atomic percentages and bandgap energies (in eV) for the three BCN sample sets

SBCN			NSBCN-BA			NSBCN-AB		
Sample	B% (avg ± stdev)	BG (eV)	Sample	B% (avg ± stdev)	BG (eV)	Sample	B% (avg ± stdev)	BG (eV)
0 mmol	0	2.52	0 mmol	0	2.33	0 mmol	0	1.94
1 mmol	0.75 ± 0.01	2.57	1 mmol	4.88 ± 0.98	1.86	0.64 mmol	4.84 ± 0.42	1.94
2 mmol	1.33 ± 0.23	2.34	2 mmol	5.50 ± 0.25	1.82	3.20 mmol	8.13 ± 0.45	1.74
3 mmol	1.61 ± 0.29	2.53	3 mmol	7.90 ± 0.45	2.01	6.40 mmol	17.41 ± 0.11	1.67
			6 mmol	22.85 ± 0.17	2.80			

 This journal is © The Royal Society of Chemistry 2023

Published on 05 December 2023. Downloaded by Duke University on 12/13/2023 5:24:52 PM.

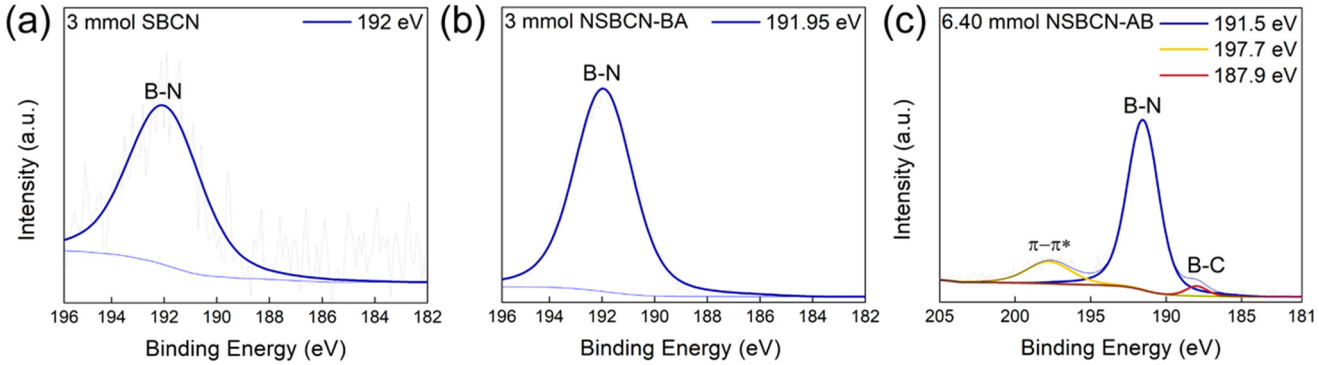

Fig. 2 B 1s peak deconvolution in (a) 3 mmol SBCN, (b) 3 mmol NSBCN-BA, and (c) 6.4 mmol NSBCN-AB. These samples were chosen as they are the highest-doped samples (considered for further characterization) from each synthesis route and showcase the maximum possible extent of boron doping in this study. All other B 1s spectra are included in Tables S6–S8,† under the B 1s columns.

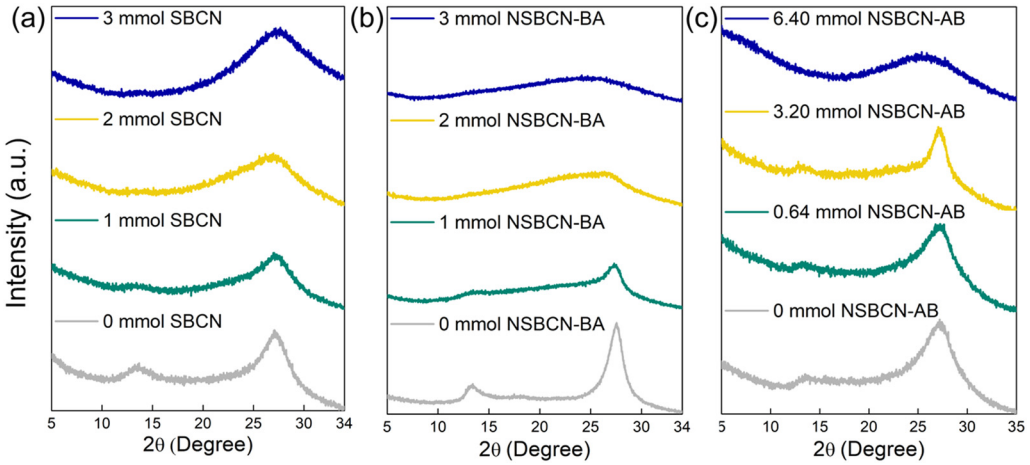

Fig. 3 XRD diffractograms for (a) S-BCN set, (b) NS-BCN-BA set, (c) NS-BCN-AB set.

three sample sets (Fig. 3) indicate the presence of the characteristics peaks for carbon nitride at 2θ = 13° (representing the tri-*s*-triazine unit[27,30,38,44]) and 27° (representing interlayer stacking[27,30,38,44]). The changes in these characteristic peaks, including peak broadening and diminished intensity, are indicative of interlayer distortion (*e.g.*, exfoliation, reduced layer thickness). For SBCN samples (Fig. 3a), the 13° peak disappears at B precursor amounts greater than 1 mmol, and the intensity of the 27° peak decreases with increasing doping levels. Similar trends are seen for the non-supramolecular sample sets NSBCN-BA (Fig. 3b) and NSBCN-AB (Fig. 3c). The reduction in peak intensities is attributed to boron atoms interfering with the two-dimensional, layered carbon-nitride structure, which deforms the interlayer stacking order. The XRD results of the supramolecular sample set show relatively invariable peak intensity for the 27° peak across the sample set. This suggests a higher preserved local order of the pristine g-CN structure. The higher-order is attributed to the tendency of SBCN's melamine–cyanuric acid complex (formed *in situ* during calcination)[26] to comprise three melamine molecules in the same plane in the formation of the tri-*s*-triazine unit. There is a consistent peak distortion of the 27° peak in the NSBCN-BA sample set with an increase in doping. There is less distortion in the 27° peak until the 3.20 mmol of the NSBCN-AB sample set. These varying observations across the two non-supramolecular approaches imply the possible role of different precursors (*i.e.*, melamine and boric acid in NSBCN-BA *versus* dicyandiamide and ammonia borane in NSBCN-AB) in the way boron doping interferes with the interlayer stacking of carbon nitride.

3.3. Synthesis method influences BCN morphology

Transmission electron spectroscopy (TEM) illuminates the morphological characteristics of the BCN samples synthesized under different conditions, and electron energy loss spectroscopy (EELS) reveals the elemental distribution across the synthesized samples (Fig. 4). The supramolecular approach (SBCN, using boric acid as B precursor) resulted in exfoliated samples with an increase in porosity as the molar ratio of the B dopant increases (Fig. 5a and b). Porosity in g-CN emerges from

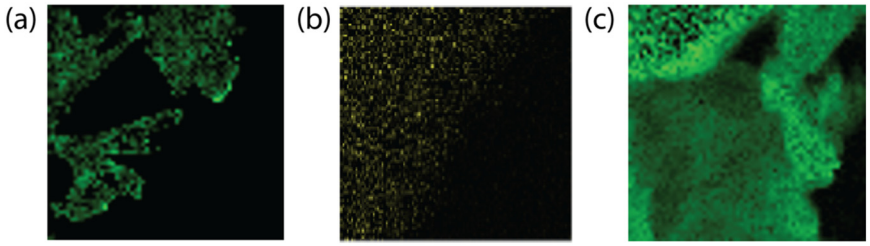

Fig. 4 EELS of (a) 3 mmol SBCN, (b) 6 mmol NSBCN-BA, (c) 6.40 mmol NSBCN-AB. Green indicates B atom location within the BCN sheet.

Published on 05 December 2023. Downloaded by Duke University on 12/13/2023 5:24:52 PM.

the release of gases, such as CO_2, NH_3, and CO, during the high-temperature calcination step of the synthesis.[47] Increased porosity for BCN has been observed by Mahvelati-Shamsabadi, *et al.*,[48] and is believed to emerge from the decomposition of the boric acid molecule into H_2O gas. Increased porosity can provide more active sites on the BCN surface for chemical reactions and facilitate efficient transfer of charges between the reaction molecules, particularly in applications such as photocatalysis.[47,49] The non-supramolecular synthesis with ammonia borane (NSBCN-AB, Fig. 5e and f) resulted in a similar porous morphology, having a curled sheet structure with round edges. For the non-supramolecular synthesis with boric acid (NSBCN-BA, Fig. 5c and d), the TEM analysis reveals a different morphology resembling a sheet structure with distinct edges. The stacked nanosheet thickness appears to increase (less transparent) with increased doping, which is corroborated by the XRD results. The observed peak distortion for the $2\theta = 27°$ peak in the NSBCN-BA and NSBCN-AB samples with increased B doping % indicates deformed interlayer stacking, which can influence the observed nanosheet thickness.

3.4. Boron doping influences the optical properties of carbon nitride

3.4.1. Modulating boron atomic percentages influence the optical bandgap. The optical bandgap (or band gap energy, E_{gap}) of a semiconducting material is the energy required to transition an electron from its valence band to the conduction band. Upon reaching the conduction band, the electron can move freely in the crystal lattice and serve as a charge carrier. The E_{gap} (in eV, Table 1) of the synthesized samples was determined from measured UV-vis-DRS data *via* Tauc plots (Fig. S2†). There is a negligible change in E_{gap} observed in S-BCN samples (Table 1), despite there being a minor difference of 0.86 atomic % (between 0 mmol SBCN and 3 mmol SBCN) doping. There is a gradual decrease in the band gap of the NSBCN-BA sample set with increased doping until 3 mmol, when the E_{gap} increases. This increasing trend is maintained for the 6 mmol sample. The bandgap increment for higher B doped samples (*i.e.*, 3 mmol and 6 mmol NSBCN-BA) is on account of the quantum confinement effect introduced by the presence of higher B atoms in the g-CN framework.[39]

Conversely, there is a consistent decreasing trend of optical bandgap observed for the NSBCN-AB samples. The band gap of inorganic semiconductor materials has been found to narrow with increasing structural defects.[50] Additionally, our PL spectra (*vide infra*, Fig. 6) of the NSBCN-AB sample set reveal a difference in photoluminescence peak intensities (*i.e.*, intensity increases for NSBCN-AB samples) with increasing B doping, which is influenced by the structural defects generated.[50] This suggests that the

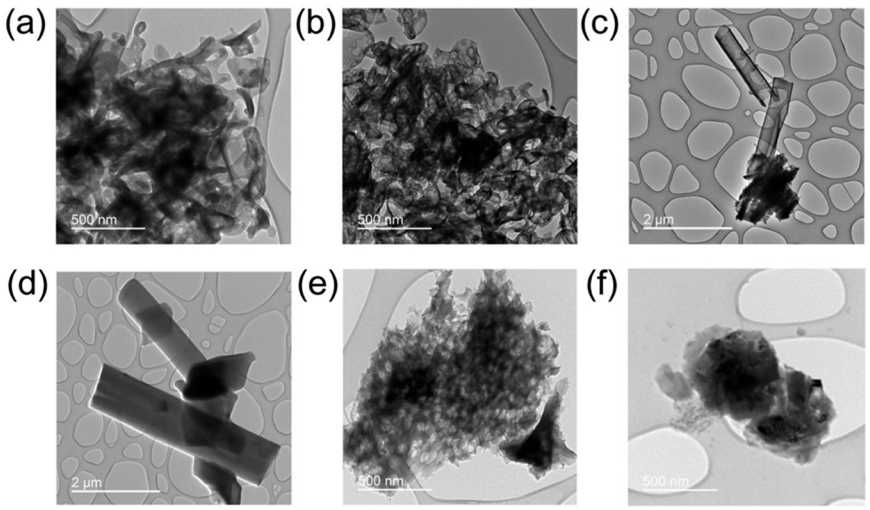

Fig. 5 TEM images of: (a) 0 mmol S-BCN, (b) 3 mmol S-BCN, (c) 0 mmol NSBCN-BA, (d) 6 mmol NSBCN-BA, (e) 0 mmol NSBCN-AB, (f) 6.40 mmol NSBCN-AB. Note: the scale bar for (e) and (f) is 500 nm.

 This journal is © The Royal Society of Chemistry 2023

Published on 05 December 2023. Downloaded by Duke University on 12/13/2023 5:24:52 PM.

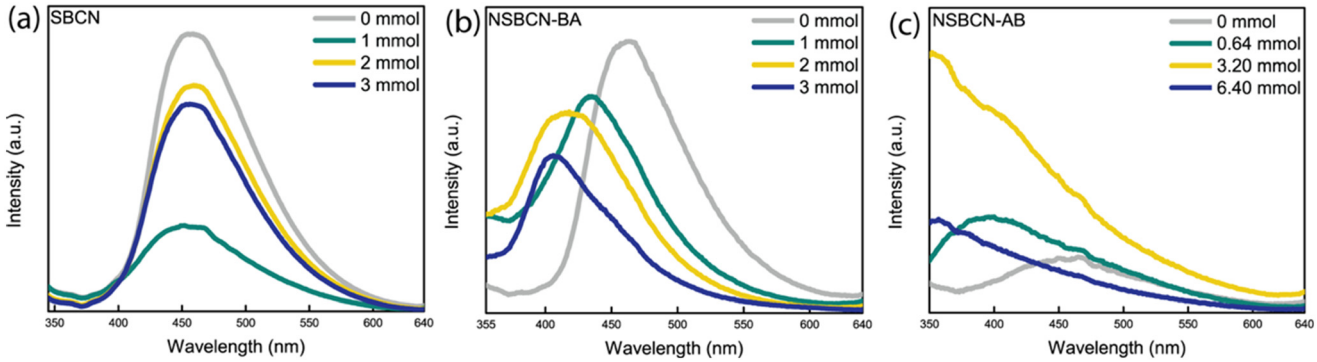

Fig. 6 Photoluminescence spectra for: (a) S-BCN, (b) NSBCN-BA, (c) NSBCN-AB.

Table 2 Summary of bandgaps found in the B-doped carbon nitride literature

Study	Boron Precursors	Optical bandgap range (in eV)
BCN for photocatalytic UO_2^{2+} reduction[51]	Boric acid	2.49–2.57
BCN for photocatalytic degradation of organic dyes[52]	Diboron trioxide	2.61–2.75
BCN for photocatalytic water splitting[53]	Ammoniotrihydroborate	2.55–2.68
BCN for photocatalytic NO_x removal[44]	Boric acid	2.54–2.70
BCN synthesized in this work	Boric acid and Ammonia borane	1.67–2.52

lowering of bandgap in the NSBCN-AB sample set is due to the doping-induced structural defects. The optical bandgap range observed in this work is compared to the BCN optical bandgap ranges in some previous research studies (Table 2). An important advancement in our work, synthesizing BCN using various approaches, is the observation of the lower bound of the bandgap range shifting further into the region conducive to visible light.

3.4.2. The approach to boron doping differentially influences electron–hole recombination. Charge separation reflects the ability of electrons and holes to remain separated. This is essential for photocatalytic applications of g-CN, where electrons and holes play a critical role in generating reactive oxidative species. Photoluminescence (PL) spectroscopy elucidates the charge separation efficiency. The intensity of PL peaks signifies the intensity of light emission exhibited by the photon released when an electron and hole pair undergo recombination. The greater the peak intensity, the greater the electron–hole recombination.[27]

The PL peak intensities for SBCN (Fig. 6a) and NSBCN-AB (Fig. 6c) do not trend with atomic % B. Notably, the 1 mmol SBCN sample and the 6.40 mmol NSBCN-AB sample exhibit reduced recombination compared with the other samples in their respective sets, as indicated by the lower-than-expected intensity. For SBCN, the multiple PL runs (*i.e.*, three independent attempts to disperse each sample in a solvent and measuring PL intensities every time) returned different trends in relative intensity, suggesting heterogeneity in doping across the BCN samples prepared *via* the supramolecular method. For the 6.40 mmol NSBCN-AB sample, we believe the departure from the trend could emerge from the saturation of doping sites or the amount of ammonia borane is so high that it uniquely interferes with the tri-*s*-triazine bond formation.

There are notable blue-shifts (*i.e.*, peak shifts towards lower wavelengths) in the non-supramolecular sample sets: NSBCN-BA (Fig. 6b) and NSBCN-AB (Fig. 6c). The blue shift is ascribed to the interlayer strain and the quantum confinement effect induced by boron doping.[39,54] The PL intensity of NSBCN-BA is observed to decrease with an increase in atomic % B, suggesting relatively low recombination with increased doping. This differing trend in recombination could emerge from the differences in morphology with the distinct edges providing charge-trapping or recombination sites (Fig. 5c and d). Combined, these observations illuminate the importance of material structure variations generated during synthesis, and influenced by different doping regimens, on photocatalytic properties of g-CN.

3.5. Life cycle assessment to capture environmental impacts of different synthesis approaches

With growing research interest in g-CN, there is a critical opportunity to inform and direct its development in a way that is minimally impactful. Life cycle impact assessment (LCIA) is an established methodology that can be used to quantify environmental impacts associated with any material. Previous LCIAs of engineered nanomaterials identify energy demand from raw material extraction and synthesis processes as the predominant contributor to environmental impacts.[55–57] Given that we achieve a range of physicochemical properties through B doping and use different synthesis methods, including varying processes and precursors, we employ LCIA to (i) identify high-impact components of BCN production, (ii) determine environmental impact tradeoffs of our synthesis routes, and (iii) elucidate possible avenues to reduce the environmental footprint. Taking these cradle-to-gate (*i.e.*, raw

Published on 05 December 2023. Downloaded by Duke University on 12/13/2023 5:24:52 PM.

material acquisition through synthesis) impacts and the physical–chemical properties of each BCN material together, we can quantitatively compare the performance and environmental tradeoffs.

LCIA was conducted for the production of 1 g of BCN *via* the two synthesis approaches and two boron precursors (Fig. 8). The synthesis processes were divided into four categories: electricity to power the reactor, chemical reagents, precursors, and synthesis-associated emissions. Each was analyzed according to the nine TRACI impact categories: (i) Global Warming Potential (GWP); (ii) Photochemical Smog (PS); (iii) Acidification (AD); (iv) Eutrophication (EU); (v) Carcinogenics (CA); (vi) Non carcinogenics (NC); (vii) Respiratory Effects (RE); (viii) Ecotoxicity (EC); (ix) Fossil Fuel Depletion (FF). Since each category has a unique unit, the impacts are presented for each category as the relative contribution of the four categories (Fig. 7a–c). The combined results indicate that synthesis-related energy demand is the greatest contributor to the impacts regardless of the approach. Further, the approaches are plotted together on a relative basis to compare the total impacts of the three synthesis methods (Fig. 7d).

Across the three synthesis methods, electricity contributes the greatest percent contribution (>87%) to the overall impact for every TRACI impact category. The electricity source assumed in this analysis was 'Electricity country mix – Low Voltage – Electricity, at grid, US/US'. This electricity source consists of electricity generation from multiple fuel sources: biomass, coal, petroleum, geothermal, natural gas, nuclear, solar, hydroelectric, and wind energy sources. An in-depth analysis of electricity impacts in SimaPro revealed that sources such as bituminous coal, natural gas, and lignite coal in the mix were the primary impact components. While the energy demand per mass of BCN produced may decrease as production scales up,[58–60] energy demand is likely to remain the predominant component of material synthesis impacts. Thus, a potential strategy to reduce the impact of energy demand during BCN syntheses is to adopt an electricity source with minimal fossil fuel.

The reagents are another contributor to the overall impacts, particularly in SBCN synthesis (Fig. 7a). The solvents used in the syntheses are ethanol (SBCN, Fig. 7a) and deionized water (NSBCN-BA, Fig. 7b, and NSBCN-AB, Fig. 7c). The range in percent contribution attributed to ethanol (the only reagent used in this synthesis) in SBCN synthesis varies between 3–17% in the EU, HHC, HHNC, EC, and FF categories. Although ethanol is considered a green solvent,[61–63] these results – comparing Fig. 7a–c – importantly highlight the benefit of using water, whenever possible, as the solvent used in chemical processes.

Among the three synthesis approaches, SBCN production has the highest relative impact across all the TRACI impact categories considered in this investigation (Fig. 7d). The high impact of SBCN production emerges from the utility of an extra precursor (*i.e.*, cyanuric acid, which was employed to form the melamine–cyanuric supramolecular complex) and an additional processing step (*i.e.*, bath sonication).

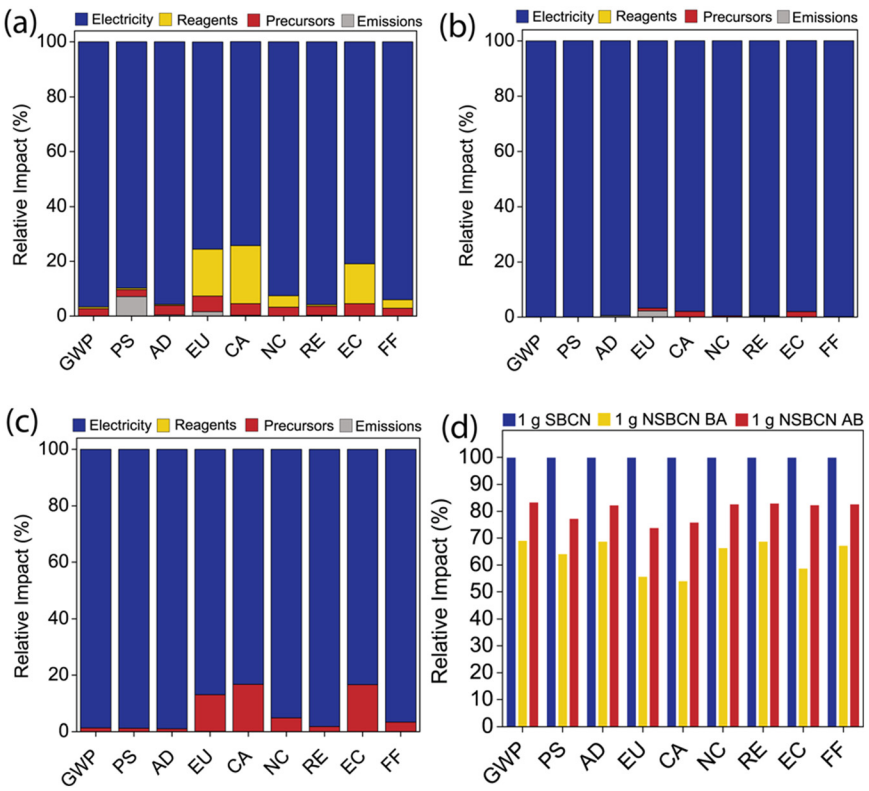

Fig. 7 Process contributions associated with the nine TRACI impact categories to produce 1 g of (a) 1 mmol SBCN, (b) 1 mmol NSBCN-BA, and (c) 0.64 mmol NSBCN-AB; and (d) the relative impact assessment for synthesizing 1 g of BCN using the three synthesis methods.

 This journal is © The Royal Society of Chemistry 2023

Published on 05 December 2023. Downloaded by Duke University on 12/13/2023 5:24:52 PM.

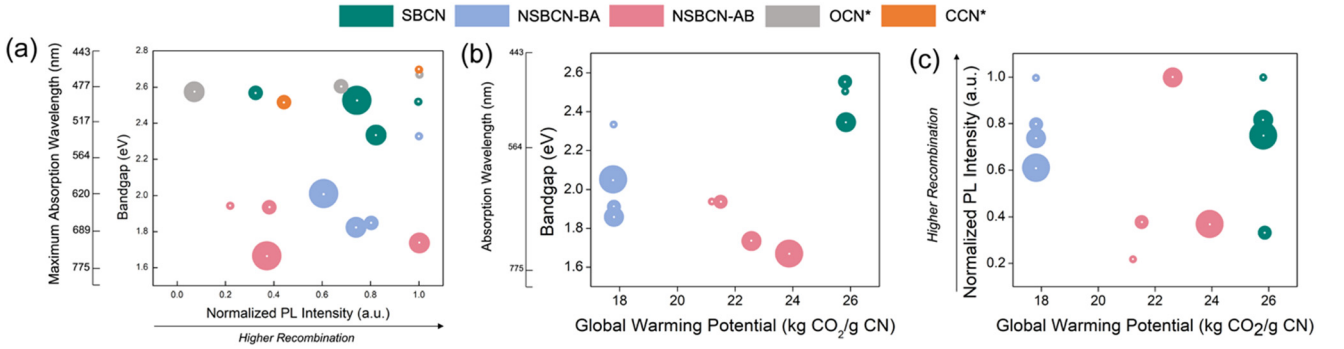

Fig. 8 Example MAPS plots showing, (a) optical bandgap and photoluminescence intensity tradeoffs for the synthesized BCN samples sets along with OCN[64] and CCN[65] sample sets, (b) tradeoffs between optical bandgap with the global warming potential associated with different g-CN synthesis methods (this plot shares the maximum absorption wavelength *y*-axis scale with plot (a)), and (c) tradeoffs between the photoluminescence intensity and the synthesis method's global warming potential. The size of the colored circles is proportional to the heteroatom atomic % dopant (B, O, or C). The center white dots represent the data point associated with the *x*–*y* coordinates.

Moreover, for impact categories such as smog formation and eutrophication potential in the SBCN production (Fig. 7a), a considerable relative impact contribution of synthesis emissions was observed. These synthesis emissions are likely on account of isocyanic acid, which is an emission associated with cyanuric acid precursor employed in the SBCN synthesis.

3.6. Design of graphitic carbon nitride that considers physicochemical property and environmental impact metrics

With near infinite possibilities for synthesizing new materials, the knowledge informing how to narrow the design space to achieve desired properties for specific applications holds immense value. Equally critical is determining whether it is possible to achieve equivalent functional performance with a lower environmental impact through choices made at the material inception (*i.e.*, at synthesis). We propose a Material Properties and Sustainability (or MAPS) approach (Fig. 8), which includes simultaneous consideration of relevant environmental impact metrics (here, using the global warming potential, kg CO_2) and physicochemical properties of g-CN, such as bandgap energy (in eV) and photoluminescence light intensity (normalized arbitrary units, A.U.; details in Section S6† for calculating the normalized arbitrary units for PL intensities), that underline photocatalytic performance. In this way, we compare g-CN options for achieving performance goals and elucidate environmental impact tradeoffs (or lack thereof) within the potential design space. To illustrate the versatility of these MAPS plots, we include g-CN materials synthesized and characterized by researchers for these same performance properties; one example of oxygen-doped carbon nitride (OCN)[64] and carbon-doped carbon nitride (CCN).[65] The adaptability across functional properties is straightforward, given the universal metrics adopted for primary g-CN properties. We are unable to include these samples in the MAPS plots that include our environmental impact unit (GWP), which elucidates an opportunity and need within the advanced material research community (*vide infra*).

The optical band gap, the associated maximum wavelength of absorption (nanometer, nm), and the photoluminescence peak are material properties that represent critical optical performance properties for wide-ranging applications of g-CN. Lower photoluminescence intensity indicates less electron–hole recombination, enhancing the potential for radical oxidative species generation, which is critical for downstream reactions underlining photocatalysis and water splitting. Optical band gap is directly related to the energy of light absorbed, thus reducing the bandgap allows for absorbance of longer, lower energy, visible light. We have chosen GWP as a representative environmental impact metric because it is commonly used across the LCA literature and, while the magnitude of impacts change between categories, the relative impacts will be similar (plots including additional environmental impact categories are included in Fig. S4†). Minimizing GWP of synthesis is desired, as it indicates a lower environmental impact. Keeping the above information in mind, the MAPS plots (Fig. 8) provide insights into the associated tradeoffs and thus, can assist in selecting g-CN materials that meet the desired criteria for specific applications while informing the potential to simultaneously reduce the material's embodied resource footprint. Specific constraints and desired threshold values for band gap and PL intensity will vary by specific application. For many environmental applications, the lower band gap is desired to attain efficiency at harvesting lower energy (higher wavelength) visible light (as opposed to high energy UV, for example). While PL intensity on its own does not comprehensively represent the intricacies of light interacting with g-CN to produce reactive oxygen species, in general, lower recombination is desired. This would direct us to options in the lower left side of the MAPS plot, Fig. 8a. In this example, we would be choosing between three samples synthesized using the non-supramolecular approach and ammonia borane precursor. The specific sample chosen would depend on how the specific tradeoffs influence performance considering the entire system of a given application.

Published on 05 December 2023. Downloaded by Duke University on 12/13/2023 5:24:52 PM.

Considering these properties alongside GWP (Fig. 8b and c) aids in further honing the optimal alternative(s). Considering band gap and GWP (Fig. 8b) there is a clear tradeoff if the lowest band gap energy is desired. The ammonia borane samples sacrifice approximately 4 kg CO_2 g^{-1} CN compared with the boric acid samples (NSBCN-BA) (note: ammonia borane is not available in SimaPro's databases, thus the process was established by the authors based on a patent,[66] which is why the GWP varies slightly compared with BCN samples prepared using reagents available in the databases.). Considering electron–hole recombination, the 1 mmol and 2 mmol NSBCN-AB outperform the alternatives. While the conclusions from these MAPS plots may ultimately lead to a performance-environmental impact tradeoff, the material or product designer enters the development process equipped with concrete guidance enabling an informed decision.

Expanding these plots to include additional alternatives (*e.g.*, with other heteroatom dopants, other modifications to manipulate properties linked to material performance) will facilitate sustainable development of g-CN applications, which pertain to clean energy harvesting, storage, water decontamination, among others. Solving these grand challenges must be pursued with solutions that are holistically sustainable to avoid shifting burdens between life cycle stages and unintended consequences. One critical limitation precluding inclusion of additional g-CN samples (*e.g.*, OCN and CCN samples in Fig. 8a) pertains to variability in the underlying assumptions across LCA studies and lack of standardization in reporting across synthesis reports. For example, Aquino de Carvalho, *et al.*[67] assumed 100% yield in their LCIA of various g-CN syntheses due to the lack of yield data reported. Here, we include our actual yield for our BCN samples prepared, thus preventing a fair GWP comparison across samples.

4.0 Conclusion

The demand for design and production of new materials is concomitant with technological and societal advances. Further, materials will underline transformative solutions to our global grand challenges and thus, must avoid introducing embodied and direct adverse implications on the environment and human health. Advances in materials science and engineering thus, must co-occur with considerations of their impact early in the design phase. In addition to reporting on novel synthetic approaches to dope graphitic carbon nitride with varying degrees of B, the study herein presents a framework for how these multiple objectives can be successfully pursued. Given the demonstrated ability to modulate properties critical for applications *via* B doping, this work evokes new directions in g-CN design and synthesis.

Synthesizing BCN using multiple approaches and dopant precursors illuminated that increasing boron doping percentage introduces structural defects that modulate the optical properties of BCN. These defects lead to bandgap energy reduction; however, we find that this reduction does not correlate with the suppression of electron–hole recombination. SBCN sample set shows inconsistency in variation of both bandgap and electron–hole recombination. NSBCN-BA shows a decrease in band gap with doping along with reduced electron–hole recombination. NSBCN-AB experiences a band gap reduction with doping, but an increase in electron–hole pair recombination. These findings suggest that the structural defects introduced by doping can act as charge-trapping sites in NSBCN-BA and recombination centers in NSBCN-AB. Exploring BCN morphological variations shed light on possible explanations for the synthesis-induced variations in g-CN optical properties. However, further investigations on the dynamic behavior of g-CN-associated photocatalysis are encouraged by employing techniques such as time-resolved transient absorption spectra analysis and transient PL spectrum.

Our LCIA results demonstrate that electricity is the major contributor to the overall impacts of BCN synthesis, regardless of the synthesis technique used. The results further emphasize the importance of minimizing precursors and processing steps during g-CN synthesis to reduce the associated environmental footprint. The introduced MAPS plot approach combines critical material metrics for performance and environmental impact, allowing visualization and quantitative tradeoff evaluation between material alternatives. This approach aims to guide the community in making informed decisions about material design and synthesis.

Conflicts of interest

There are no conflicts to declare.

Acknowledgements

Y. S. and L. M. G. acknowledge the funding support from the National Science Foundation CAREER Grant (CBET No. 2039823). The authors extend their sincere appreciation to Dr. Paul Leu, Mingxuan Li, and Mehdi Zarei for their invaluable assistance with UV-vis DRS measurements. Special thanks go to Dr. Susheng Tan for conducting TEM analyses and providing valuable insights. Sincere thanks to the laboratory manager Dr. David Malehorn assistance maintaining the research equipment. The authors also express their gratitude to Dr. David Waldeck and Nazifa Tabassum for their assistance with ss-PL measurements and for engaging in constructive discussions. The authors would like to acknowledge the Nanoscale Fabrication and Characterization Facility as well as the Material Characterization Laboratory at the University of Pittsburgh for providing access to the material characterization facilities that greatly facilitated this research.

 This journal is © The Royal Society of Chemistry 2023

Published on 05 December 2023. Downloaded by Duke University on 12/13/2023 5:24:52 PM.

References

1 Global Nanotechnology Market Outlook & Growth Forecast Report. https://www.bccresearch.com/market-research/nanotechnology/global-nanotechnology-market.html (accessed 2023-09-07).

2 S.-F. Ng, X. Chen, J. J. Foo, M. Xiong and W.-J. Ong, 2D Carbon Nitrides: Regulating Non-Metal Boron-Doped C3N5 for Elucidating the Mechanism of Wide PH Range Photocatalytic Hydrogen Evolution Reaction, *Chin. J. Catal.*, 2023, **47**, 150–160, DOI: 10.1016/S1872-2067(23)64417-1.

3 A. Mishra, A. Mehta, S. Basu, N. P. Shetti, K. R. Reddy and T. M. Aminabhavi, Graphitic Carbon Nitride (g–C3N4)–Based Metal-Free Photocatalysts for Water Splitting: A Review, *Carbon*, 2019, **149**, 693–721, DOI: 10.1016/j.carbon.2019.04.104.

4 L. Chen and J. Song, Tailored Graphitic Carbon Nitride Nanostructures: Synthesis, Modification, and Sensing Applications, *Adv. Funct. Mater.*, 2017, **27**(39), 1702695, DOI: 10.1002/adfm.201702695.

5 L. Jiang, X. Yuan, Y. Pan, J. Liang, G. Zeng, Z. Wu and H. Wang, Doping of Graphitic Carbon Nitride for Photocatalysis: A Review, *Appl. Catal., B*, 2017, **217**, 388–406, DOI: 10.1016/j.apcatb.2017.06.003.

6 M. Aleksandrzak, M. Jedrzejczak-Silicka, K. Sielicki, K. Piotrowska and E. Mijowska, Size-Dependent in Vitro Biocompatibility and Uptake Process of Polymeric Carbon Nitride, *ACS Appl. Mater. Interfaces*, 2019, **11**(51), 47739–47749, DOI: 10.1021/acsami.9b17427.

7 M. Aggarwal, S. Basu, N. P. Shetti, M. N. Nadagouda, E. E. Kwon, Y.-K. Park and T. M. Aminabhavi, Photocatalytic Carbon Dioxide Reduction: Exploring the Role of Ultrathin 2D Graphitic Carbon Nitride (g-C3N4), *Chem. Eng. J.*, 2021, **425**, 131402, DOI: 10.1016/j.cej.2021.131402.

8 B. Xu, M. B. Ahmed, J. L. Zhou, A. Altaee, G. Xu and M. Wu, Graphitic Carbon Nitride Based Nanocomposites for the Photocatalysis of Organic Contaminants under Visible Irradiation: Progress, Limitations and Future Directions, *Sci. Total Environ.*, 2018, **633**, 546–559, DOI: 10.1016/j.scitotenv.2018.03.206.

9 H. Li, Y. Liu, X. Gao, C. Fu and X. Wang, Facile Synthesis and Enhanced Visible-Light Photocatalysis of Graphitic Carbon Nitride Composite Semiconductors, *ChemSusChem*, 2015, **8**(7), 1189–1196, DOI: 10.1002/cssc.201500024.

10 J. Xu, Z. Wang and Y. Zhu, Enhanced Visible-Light-Driven Photocatalytic Disinfection Performance and Organic Pollutant Degradation Activity of Porous g-C3N4 Nanosheets, *ACS Appl. Mater. Interfaces*, 2017, **9**(33), 27727–27735, DOI: 10.1021/acsami.7b07657.

11 A. Hayat, J. A. Shah Syed, A. G. Al-Sehemi, K. S. El-Nasser, T. A. Taha, A. A. Al-Ghamdi, M. A. Amin, Z. Ajmal, W. Iqbal, A. Palamanit, D. I. Medina, W. I. Nawawi and M. Sohail, State of the Art Advancement in Rational Design of G-C3N4 Photocatalyst for Efficient Solar Fuel Transformation, Environmental Decontamination and Future Perspectives, *Int. J. Hydrogen Energy*, 2022, **47**(20), 10837–10867, DOI: 10.1016/j.ijhydene.2021.11.252.

12 G. Liao, Y. Gong, L. Zhang, H. Gao, G.-J. Yang and B. Fang, Semiconductor Polymeric Graphitic Carbon Nitride Photocatalysts: The "Holy Grail" for the Photocatalytic Hydrogen Evolution Reaction under Visible Light, *Energy Environ. Sci.*, 2019, **12**(7), 2080–2147, DOI: 10.1039/C9EE00717B.

13 A. Naseri, M. Samadi, A. Pourjavadi, A. Z. Moshfegh and S. Ramakrishna, Graphitic Carbon Nitride (g-C3N4)-Based Photocatalysts for Solar Hydrogen Generation: Recent Advances and Future Development Directions, *J. Mater. Chem. A*, 2017, **5**(45), 23406–23433, DOI: 10.1039/C7TA05131J.

14 M. Aleksandrzak, W. Kukulka and E. Mijowska, Graphitic Carbon Nitride/Graphene Oxide/Reduced Graphene Oxide Nanocomposites for Photoluminescence and Photocatalysis, *Appl. Surf. Sci.*, 2017, **398**, 56–62, DOI: 10.1016/j.apsusc.2016.12.023.

15 A. Du, S. Sanvito, Z. Li, D. Wang, Y. Jiao, T. Liao, Q. Sun, Y. H. Ng, Z. Zhu, R. Amal and S. C. Smith, Hybrid Graphene and Graphitic Carbon Nitride Nanocomposite: Gap Opening, Electron–Hole Puddle, Interfacial Charge Transfer, and Enhanced Visible Light Response, *J. Am. Chem. Soc.*, 2012, **134**(9), 4393–4397, DOI: 10.1021/ja211637p.

16 S. Singla, S. Sharma, S. Basu, N. P. Shetti and K. R. Reddy, Graphene/Graphitic Carbon Nitride-Based Ternary Nanohybrids: Synthesis Methods, Properties, and Applications for Photocatalytic Hydrogen Production, *FlatChem*, 2020, **24**, 100200, DOI: 10.1016/j.flatc.2020.100200.

17 H. Lin, J. Wu, F. Zhou, X. Zhao, P. Lu, G. Sun, Y. Song, Y. Li, X. Liu and H. Dai, Graphitic Carbon Nitride-Based Photocatalysts in the Applications of Environmental Catalysis, *J. Environ. Sci.*, 2023, **124**, 570–590, DOI: 10.1016/j.jes.2021.11.017.

18 L. Lu, Z. Lv, Y. Si, M. Liu and S. Zhang, Recent Progress on Band and Surface Engineering of Graphitic Carbon Nitride for Artificial Photosynthesis, *Appl. Surf. Sci.*, 2018, **462**, 693–712, DOI: 10.1016/j.apsusc.2018.08.131.

19 Q. Guo, Y. Zhang, J. Qiu and G. Dong, Engineering the Electronic Structure and Optical Properties of G-C_3N_4 by Non-Metal Ion Doping, *J. Mater. Chem. C*, 2016, **4**(28), 6839–6847, DOI: 10.1039/C6TC01831A.

20 Y. Liu, Y. Zheng, W. Zhang, Z. Peng, H. Xie, Y. Wang, X. Guo, M. Zhang, R. Li and Y. Huang, Template-Free Preparation of Non-Metal (B, P, S) Doped g-C3N4 Tubes with Enhanced Photocatalytic H2O2 Generation, *J. Mater. Sci. Technol.*, 2021, **95**, 127–135, DOI: 10.1016/j.jmst.2021.03.025.

21 L. K. Putri, B.-J. Ng, W.-J. Ong, H. W. Lee, W. S. Chang and S.-P. Chai, Engineering Nanoscale p–n Junction *via* the Synergetic Dual-Doping of p-Type Boron-Doped Graphene Hybridized with n-Type Oxygen-Doped Carbon Nitride for Enhanced Photocatalytic Hydrogen Evolution, *J. Mater. Chem. A*, 2018, **6**(7), 3181–3194, DOI: 10.1039/C7TA09723A.

22 O. Stephan, P. M. Ajayan, C. Colliex, Ph. Redlich, J. M. Lambert, P. Bernier and P. Lefin, Doping Graphitic and Carbon Nanotube Structures with Boron and Nitrogen,

Published on 05 December 2023. Downloaded by Duke University on 12/13/2023 5:24:52 PM.

Science, 1994, **266**(5191), 1683–1685, DOI: **10.1126/science.266.5191.1683**.

23 L. Chen, Y. Wang, S. Cheng, X. Zhao, J. Zhang, Z. Ao, C. Zhao, B. Li, S. Wang, S. Wang and H. Sun, Nitrogen Defects/Boron Dopants Engineered Tubular Carbon Nitride for Efficient Tetracycline Hydrochloride Photodegradation and Hydrogen Evolution, *Appl. Catal., B*, 2022, **303**, 120932, DOI: **10.1016/j.apcatb.2021.120932**.

24 R. Jiang, M. Jiang, Z. Huang, J. Wang, Y. Kuang and C. Fu, Constructing Light-Weight Polar Boron-Doped Carbon Nitride Nanosheets with Increased Active Sites and Conductivity for High Performance Lithium-Sulfur Batteries, *Int. J. Hydrogen Energy*, 2020, **45**(29), 14940–14952, DOI: **10.1016/j.ijhydene.2020.03.232**.

25 D. Peng, W. Jiang, F.-F. Li, L. Zhang, R.-P. Liang and J.-D. Qiu, One-Pot Synthesis of Boron Carbon Nitride Nanosheets for Facile and Efficient Heavy Metal Ions Removal, *ACS Sustainable Chem. Eng.*, 2018, **6**(9), 11685–11694, DOI: **10.1021/acssuschemeng.8b01951**.

26 M. Shalom, S. Inal, C. Fettkenhauer, D. Neher and M. Antonietti, Improving Carbon Nitride Photocatalysis by Supramolecular Preorganization of Monomers, *J. Am. Chem. Soc.*, 2013, **135**(19), 7118–7121, DOI: **10.1021/ja402521s**.

27 N. Aquino de Carvalho, Y. Wang, N. Morales-Soto, D. Waldeck, K. Bibby, K. Doudrick and L. M. Gilbertson, Using C-Doping to Identify Photocatalytic Properties of Graphitic Carbon Nitride That Govern Antibacterial Efficacy, *ACS ES&T Water*, 2021, **1**(2), 269–280, DOI: **10.1021/acsestwater.0c00053**.

28 Q. Yan, G.-F. Huang, D.-F. Li, M. Zhang, A.-L. Pan and W.-Q. Huang, Facile Synthesis and Superior Photocatalytic and Electrocatalytic Performances of Porous B-Doped g-C3N4 Nanosheets, *J. Mater. Sci. Technol.*, 2018, **34**(12), 2515–2520, DOI: **10.1016/j.jmst.2017.06.018**.

29 H. Zhao, H. Yu, X. Quan, S. Chen, Y. Zhang, H. Zhao and H. Wang, Fabrication of Atomic Single Layer Graphitic-C3N4 and Its High Performance of Photocatalytic Disinfection under Visible Light Irradiation, *Appl. Catal., B*, 2014, **152–153**, 46–50, DOI: **10.1016/j.apcatb.2014.01.023**.

30 Y. Wang, H. Li, J. Yao, X. Wang and M. Antonietti, Synthesis of Boron Doped Polymeric Carbon Nitride Solids and Their Use as Metal-Free Catalysts for Aliphatic C–H Bond Oxidation, *Chem. Sci.*, 2011, **2**(3), 446–450, DOI: **10.1039/C0SC00475H**.

31 R. M. Yadav, R. Kumar, A. Aliyan, P. S. Dobal, S. Biradar, R. Vajtai, D. P. Singh, A. A. Martí and P. M. Ajayan, Facile Synthesis of Highly Fluorescent Free-Standing Films Comprising Graphitic Carbon Nitride (g-C3N4) Nanolayers, *New J. Chem.*, 2020, **44**(6), 2644–2651, DOI: **10.1039/C9NJ05108B**.

32 U.S. Life Cycle Inventory Database. **https://www.nrel.gov/lci/index.html** (accessed 2023-09-07).

33 DATASMART Life Cycle Inventory – Long Trail Sustainability. **https://longtrailsustainability.com/services/software/datasmart-life-cycle-inventory/** (accessed 2023-09-07).

34 G. Wernet, C. Bauer, B. Steubing, J. Reinhard, E. Moreno-Ruiz and B. Weidema, The Ecoinvent Database Version 3 (Part I): Overview and Methodology, *Int. J. Life Cycle Assess.*, 2016, **21**(9), 1218–1230, DOI: **10.1007/s11367-016-1087-8**.

35 US EPA, O. Tool for Reduction and Assessment of Chemicals and Other Environmental Impacts (TRACI). **https://www.epa.gov/chemical-research/tool-reduction-and-assessment-chemicals-and-other-environmental-impacts-traci** (accessed 2023-09-07).

36 B. Zhu, L. Zhang, B. Cheng and J. Yu, First-Principle Calculation Study of Tri-s-Triazine-Based g-C3N4: A Review, *Appl. Catal., B*, 2018, **224**, 983–999, DOI: **10.1016/j.apcatb.2017.11.025**.

37 E. Kroke, M. Schwarz, E. Horath-Bordon, P. Kroll, B. Noll and A. D. Norman, Tri-s-Triazine Derivatives. Part I. From Trichloro-Tri- s -Triazine to Graphitic C 3 N 4 Structures, *New J. Chem.*, 2002, **26**(5), 508–512, DOI: **10.1039/B111062B**.

38 E. Alwin, W. Nowicki, R. Wojcieszak, M. Zieliński and M. Pietrowski, Elucidating the Structure of the Graphitic Carbon Nitride Nanomaterials *via* X-Ray Photoelectron Spectroscopy and X-Ray Powder Diffraction Techniques, *Dalton Trans.*, 2020, **49**(36), 12805–12813, DOI: **10.1039/D0DT02325F**.

39 Graphene-Like Carbon Nitride Nanosheets for Improved Photocatalytic Activities - Niu - 2012 - Advanced Functional Materials - Wiley Online Library. **https://onlinelibrary.wiley.com/doi/full/10.1002/adfm.201200922** (accessed 2023-09-08).

40 W. Lin, W. Hong, L. Sun, D. Yu, D. Yu and X. Chen, Bioinspired Mesoporous Chiral Nematic Graphitic Carbon Nitride Photocatalysts Modulated by Polarized Light, *ChemSusChem*, 2018, **11**(1), 114–119, DOI: **10.1002/cssc.201701984**.

41 M. H. Engelhard, D. R. Baer, A. Herrera-Gomez and P. M. A. Sherwood, Introductory Guide to Backgrounds in XPS Spectra and Their Impact on Determining Peak Intensities, *J. Vac. Sci. Technol., A*, 2020, **38**(6), 063203, DOI: **10.1116/6.0000359**.

42 G. H. Major, N. Fairley, P. M. A. Sherwood, M. R. Linford, J. Terry, V. Fernandez and K. Artyushkova, Practical Guide for Curve Fitting in X-Ray Photoelectron Spectroscopy, *J. Vac. Sci. Technol., A*, 2020, **38**(6), 061203, DOI: **10.1116/6.0000377**.

43 Emerging tri-s-triazine-based graphitic carbon nitride: A potential signal-transducing nanostructured material for sensor applications - Chouhan - 2021 - Nano Select - Wiley Online Library. **https://onlinelibrary.wiley.com/doi/full/10.1002/nano.202000228** (accessed 2023-09-08).

44 Z. Wang, M. Chen, Y. Huang, X. Shi, Y. Zhang, T. Huang, J. Cao, W. Ho and S. C. Lee, Self-Assembly Synthesis of Boron-Doped Graphitic Carbon Nitride Hollow Tubes for Enhanced Photocatalytic NOx Removal under Visible Light, *Appl. Catal., B*, 2018, **239**, 352–361, DOI: **10.1016/j.apcatb.2018.08.030**.

45 L. G. Jacobsohn, R. K. Schulze, M. E. H. Maia da Costa and M. Nastasi, X-Ray Photoelectron Spectroscopy Investigation of Boron Carbide Films Deposited by Sputtering, *Surf. Sci.*, 2004, **572**(2), 418–424, DOI: **10.1016/j.susc.2004.09.020**.

46 Introduction to x-ray photoelectron spectroscopy | Journal of Vacuum Science & Technology A | AIP Publishing. **https://pubs.aip.org/avs/jva/article/38/6/063204/1024200/**

 This journal is © The Royal Society of Chemistry 2023

Published on 05 December 2023. Downloaded by Duke University on 12/13/2023 5:24:52 PM.

Introduction-to-x-ray-photoelectron-spectroscopy (accessed 2023-09-08).

47 J. Wang, J. Hao, D. Liu, S. Qin, D. Portehault, Y. Li, Y. Chen and W. Lei, Porous Boron Carbon Nitride Nanosheets as Efficient Metal-Free Catalysts for the Oxygen Reduction Reaction in Both Alkaline and Acidic Solutions, *ACS Energy Lett.*, 2017, **2**(2), 306–312, DOI: **10.1021/acsenergylett.6b00602**.

48 T. Mahvelati-Shamsabadi, H. Fattahimoghaddam, B.-K. Lee, H. Ryu and J. I. Jang, Caesium Sites Coordinated in Boron-Doped Porous and Wrinkled Graphitic Carbon Nitride Nanosheets for Efficient Charge Carrier Separation and Transfer: Photocatalytic H2 and H2O2 Production, *Chem. Eng. J.*, 2021, **423**, 130067, DOI: **10.1016/j.cej.2021.130067**.

49 K. Qi, N. Cui, M. Zhang, Y. Ma, G. Wang, Z. Zhao and A. Khataee, Ionic Liquid-Assisted Synthesis of Porous Boron-Doped Graphitic Carbon Nitride for Photocatalytic Hydrogen Production, *Chemosphere*, 2021, **272**, 129953, DOI: **10.1016/j.chemosphere.2021.129953**.

50 Bandgap analysis and carrier localization in cation-disordered ZnGeN2 | APL Materials | AIP Publishing. **https://pubs.aip.org/aip/apm/article/10/1/011112/2834890/Bandgap-analysis-and-carrier-localization-in** (accessed 2023-09-08).

51 C. Lu, R. Chen, X. Wu, M. Fan, Y. Liu, Z. Le, S. Jiang and S. Song, Boron Doped G-C3N4 with Enhanced Photocatalytic UO22+ Reduction Performance, *Appl. Surf. Sci.*, 2016, **360**, 1016–1022, DOI: **10.1016/j.apsusc.2015.11.112**.

52 Y. Zhong, Y. Lin, Q. Chen, Y. Sun and F. Fu, Rapid Photo-Degradation of Various Organic Dyes with Thin-Layer Boron-Doped Graphitic Carbon Nitride Nano-Sheets under Visible Light Irradiation, *J. Environ. Chem. Eng.*, 2020, **8**(2), 103567, DOI: **10.1016/j.jece.2019.103567**.

53 S. Thaweesak, S. Wang, M. Lyu, M. Xiao, P. Peerakiatkhajohn and L. Wang, Boron-Doped Graphitic Carbon Nitride Nanosheets for Enhanced Visible Light Photocatalytic Water Splitting, *Dalton Trans.*, 2017, **46**(32), 10714–10720, DOI: **10.1039/C7DT00933J**.

54 G. Pradhan and A. K. Sharma, Anomalous Raman and Photoluminescence Blue Shift in Mono- and a Few Layered Pulsed Laser Deposited MoS2 Thin Films, *Mater. Res. Bull.*, 2018, **102**, 406–411, DOI: **10.1016/j.materresbull.2018.03.001**.

55 L. Pourzahedi and J. M. Eckelman, Comparative Life Cycle Assessment of Silver Nanoparticle Synthesis Routes, *Environ. Sci.: Nano*, 2015, **2**(4), 361–369, DOI: **10.1039/C5EN00075K**.

56 M. J. Eckelman, M. S. Mauter, J. A. Isaacs and M. Elimelech, New Perspectives on Nanomaterial Aquatic Ecotoxicity: Production Impacts Exceed Direct Exposure Impacts for Carbon Nanotoubes, *Environ. Sci. Technol.*, 2012, **46**(5), 2902–2910, DOI: **10.1021/es203409a**.

57 T. Walser, E. Demou, D. J. Lang and S. Hellweg, Prospective Environmental Life Cycle Assessment of Nanosilver T-Shirts, *Environ. Sci. Technol.*, 2011, **45**(10), 4570–4578, DOI: **10.1021/es2001248**.

58 S. Temizel-Sekeryan and A. L. Hicks, Global Environmental Impacts of Silver Nanoparticle Production Methods Supported by Life Cycle Assessment, *Resour., Conserv. Recycl.*, 2020, **156**, 104676, DOI: **10.1016/j.resconrec.2019.104676**.

59 S. Temizel-Sekeryan, F. Wu and A. L. Hicks, Global Scale Life Cycle Environmental Impacts of Single- and Multi-Walled Carbon Nanotube Synthesis Processes, *Int. J. Life Cycle Assess.*, 2021, **26**(4), 656–672, DOI: **10.1007/s11367-020-01862-1**.

60 A. Rahman, S. Kang, S. McGinnis and P. J. Vikesland, Life Cycle Impact Assessment of Iron Oxide (Fe3O4/γ-Fe2O3) Nanoparticle Synthesis Routes, *ACS Sustainable Chem. Eng.*, 2022, **10**(10), 3155–3165, DOI: **10.1021/acssuschemeng.1c05763**.

61 L. J. Diorazio, D. R. J. Hose and N. K. Adlington, Toward a More Holistic Framework for Solvent Selection, *Org. Process Res. Dev.*, 2016, **20**(4), 760–773, DOI: **10.1021/acs.oprd.6b00015**.

62 K. Tekin, N. Hao, S. Karagoz and A. J. Ragauskas, Ethanol: A Promising Green Solvent for the Deconstruction of Lignocellulose, *ChemSusChem*, 2018, **11**(20), 3559–3575, DOI: **10.1002/cssc.201801291**.

63 F. P. Byrne, S. Jin, G. Paggiola, T. H. M. Petchey, J. H. Clark, T. J. Farmer, A. J. Hunt, C. Robert McElroy and J. Sherwood, Tools and Techniques for Solvent Selection: Green Solvent Selection Guides, *Sustainable Chem. Processes*, 2016, **4**(1), 7, DOI: **10.1186/s40508-016-0051-z**.

64 Z.-F. Huang, J. Song, L. Pan, Z. Wang, X. Zhang, J.-J. Zou, W. Mi, X. Zhang and L. Wang, Carbon Nitride with Simultaneous Porous Network and O-Doping for Efficient Solar-Energy-Driven Hydrogen Evolution, *Nano Energy*, 2015, **12**, 646–656, DOI: **10.1016/j.nanoen.2015.01.043**.

65 P. Xiao, D. Jiang, T. Liu, D. Li and M. Chen, Facile Synthesis of Carbon-Doped g-C3N4 for Enhanced Photocatalytic Hydrogen Evolution under Visible Light, *Mater. Lett.*, 2018, **212**, 111–113, DOI: **10.1016/j.matlet.2017.10.079**.

66 S. T. Autrey, D. J. Heldebrant, J. C. Linehan, A. J. Karkamkar and F. Zheng, Process for Synthesis of Ammonia Borane for Bulk Hydrogen Storage. US7897129B2, 2011.

67 Comparative life cycle assessment of graphitic carbon nitride synthesis routes - Aquino de Carvalho - 2023 - Journal of Industrial Ecology - Wiley Online Library. **https://onlinelibrary.wiley.com/doi/full/10.1111/jiec.13390** (accessed 2023-09-08).